

pubs.acs.org/cm Article

# On the Dopability of Semiconductors and Governing Material Properties

Anuj Goyal, Prashun Gorai, Shashwat Anand, Eric S. Toberer, G. Jeffrey Snyder, and Vladan Stevanović\*



Cite This: Chem. Mater. 2020, 32, 4467-4480



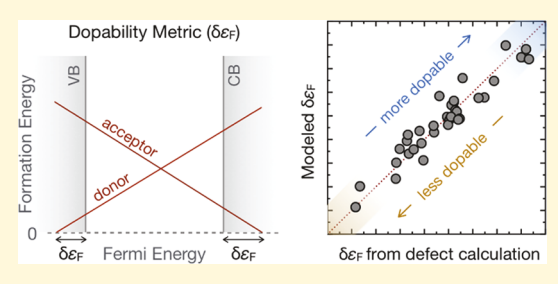
**ACCESS** 

Metrics & More

Article Recommendations

Supporting Information

ABSTRACT: To be practical, semiconductors need to be doped. Sometimes, they need to be doped to nearly degenerate levels, e.g., in applications such as thermoelectric, transparent electronics, or power electronics. However, many materials with finite band gaps are not dopable at all, while many others exhibit a strong preference toward allowing either p- or n-type doping but not both. In this work, we develop a model description of semiconductor dopability and formulate design principles in terms of governing material properties. Our approach, which builds upon the semiconductor defect theory applied to a suitably devised (tight-binding) model system, reveals analytic relationships between intrinsic material properties and the semiconductor



dopability and elucidates the role and the insufficiency of previously suggested descriptors such as the absolute band edge positions. We validate our model against a number of classic binary semiconductors and discuss its extension to more complex chemistries and the utility in large-scale material searches.

# ■ INTRODUCTION

The ability of classic semiconductors such as Si, GaAs, and PbTe to dope both p- and n-types and to achieve nearly arbitrary charge carrier concentrations is an exception rather than a rule. This is clearly illustrated by our literature survey, depicted in Figure 1. We collected the highest measured charge carrier concentrations for about 130 binary and ternary semiconductors. A number of these compounds have relatively low (maximal) reported charge carrier concentrations, and only a small fraction (36 of 130) have been successfully doped both p- and n-types. These numbers decrease significantly as the material band gap increases such that there are very few wide-gap semiconductors that are dopable at all (13 of 130 with gaps above 3 eV), with GaN being the only (weakly) ambipolar semiconductor with the band gap exceeding 3 eV. Recent predictions offer some hope that ambipolar wide-gap materials could exist, though experimental validation is still needed. 1-3 Majority (95 of 130) of the compounds from Figure 1 likely suffer from the so-called doping asymmetry, meaning that they can dope either p- or n-type but not both.

GaN is a notable example of how finding ways to overcome these doping tendencies (or bottlenecks) can be transformative. A nominally exclusively n-type semiconductor was successfully doped p-type via a rather unconventional non-equilibrium processing route that allows the insertion of acceptor-behaving Mg substitutional impurities in much higher concentrations than possible under equilibrium conditions. This accomplishment enabled the development of a blue lightemitting diode that was awarded the 2014 Nobel prize in physics. <sup>79–81</sup> Likewise, numerous attempts have been made to dope ZnO, SnO<sub>2</sub>, and In<sub>2</sub>O<sub>3</sub> p-types; <sup>82–84</sup> however, with very

little success, and to date, these compounds are regarded as exclusively n-type semiconductors. 85,86 Recent predictions suggest that the p-type doping in ZnO could be attained; however, it could not be attained in the ground-state wurtzite structure but in the metastable, high-pressure rocksalt phase. 87 Another important (counter) example is Mg<sub>3</sub>Sb<sub>2</sub>, which was, for a long time, regarded as an exclusively p-type semiconductor, a belief that was recently contested by the successful (equilibrium) n-doping followed by the demonstration of high thermoelectric performance in the n-type Mg<sub>3</sub>Sb<sub>2</sub>.<sup>88,89</sup> These doping tendencies and bottlenecks represent a critical obstacle for the discovery and design of novel functional materials, especially for applications such as thermoelectric, transparent, and power electronics where achieving nearly degenerate charge carrier concentrations is of utmost importance. 90-92

Dopability of III–V and II–VI semiconductors was investigated previously. Zunger formulated his practical doping principles as related to the formation of intrinsic compensating defects. Namely, the formation energy of any acceptor defect exhibits decreasing linear dependence on the Fermi energy ( $\varepsilon_{\rm F}$ ), while for the donors, it increases linearly with  $\varepsilon_{\rm F}$ , as shown in Figure 2. Hence, there will be a special  $\varepsilon_{\rm F}^{\rm (n)}$  value

Received: December 11, 2019 Revised: May 5, 2020 Published: May 6, 2020





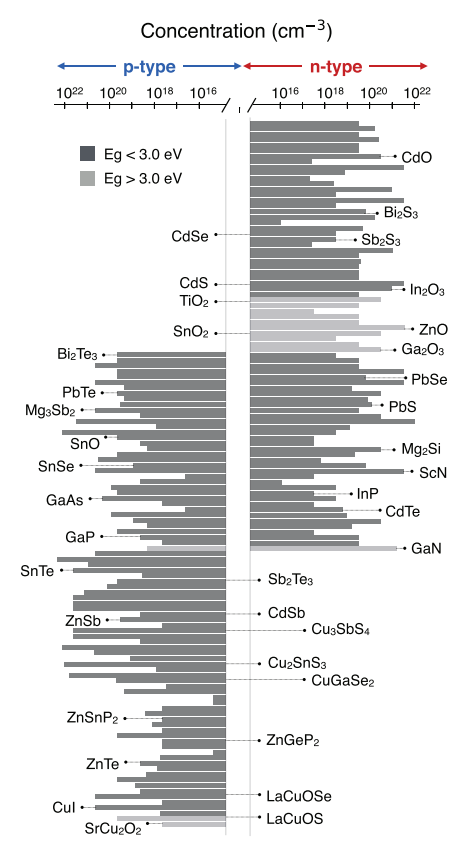


**Figure 1.** Histogram of maximal reported charge carrier concentrations for various binary and ternary semiconductors. Light and dark shades of gray distinguish the band-gap value. Data are obtained from refs 4–78, and for details, see Table S1 in the Supporting Information (S1).

above which the energy to form intrinsic acceptors becomes negative (exothermic). Similarly, there is a special  $\varepsilon_F^{(p)}$  below which the formation of intrinsic donors will be exothermic. As a consequence, any attempt to dope the system n-type by increasing  $\varepsilon_F$  beyond the  $\varepsilon_F^{(n)}$  will be met with the opposition in the form of the spontaneous formation of intrinsic acceptor (electron-compensating) defects. If  $\varepsilon_F^{(n)}$  occurs near or inside the conduction band (CB), the system will allow the introduction of electrons, and hence,  $\varepsilon_F^{(n)}$  represents a natural upper limit for n-type doping. Analogously, intrinsic donors and the resulting  $\varepsilon_F^{(p)}$  determine the limit for p-type doping.

What Zunger noticed is that within III–V and II–VI semiconductors, the n- and p-type pinning energies  $\varepsilon_{\rm F}^{(n)}$  and  $\varepsilon_{\rm F}^{(p)}$ , as he called them, obtained from defect calculations approximately align. This implies that to be dopable, the semiconductor band edges need to be close to these "universal" pinning energies. That is, the lower the conduction band minimum (CBM) position relative to the n-pinning energy, the more n-type dopable the systems are, and conversely, the higher the valence band (VB) maximum (VBM) relative to the p-pinning energy, the more p-type dopable the semiconductor is. While certainly practical, Zunger's doping principles critically rely on the empirically observed alignment of the doping pinning energies, which, as we will show later, does not hold generally for compounds outside III–V and II–VI semiconductors.

Similar design principles emerge from the consideration of another "universal" reference, the branch point energy. 94 It is

defined as the energy at which the electronic states at the surface and/or interfaces change their character from predominantly VB-like to mostly CB-like and is also used implicitly to define dopability as related to the proximity of the band edges. The lower the CBM relative to branch point energy, the more n-type dopable the system is, and the higher the VBM, the more p-type dopable the system is. If the branch point energy occurs close to the mid-gap, the system could be either ambipolar dopable or insulating. The expected universal alignment of the branch point energies between different materials then implies dopability design principles in terms of the positions of the band edges similar to those proposed by Zunger but now relative to this different reference. However, recent work shows that considerations based on the branch point energy can be used to identify n-type dopable systems much better than those of the ambipolar or the p-type systems.95

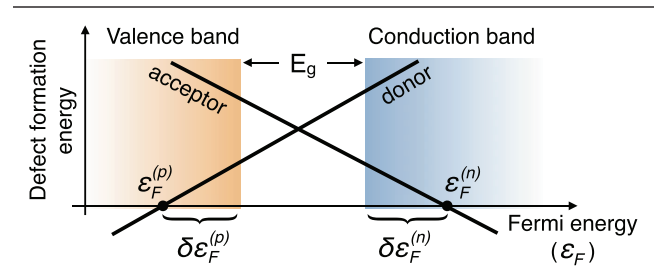


**Figure 2.** Schematic of the defect formation energy dependence on the Fermi energy for donor and acceptor defects. The "doping pinning energies" that determine the dopability of a material are denoted as  $\varepsilon_{\rm F}^{(n)}$  and  $\varepsilon_{\rm F}^{(p)}$ . In our work, we define dopability metrics  $\delta\varepsilon_{\rm F}^{(n)}$  and  $\delta\varepsilon_{\rm F}^{(p)}$  shown in the figure as deviations of the pinning energies from the corresponding band edge (see the text for details).

Also recently, Miller et al. used machine learning to develop an empirical model for dopability in diamond-like semi-conductors. While the developed model shows remarkable accuracy in reproducing and predicting achievable carrier concentrations, as with any machine learning model, its relation to the underlying physics is unclear (not causal) and the transferability beyond the diamond-like semiconductors is questionable due to the scarcity of the measured carrier concentrations needed for the model development.

Herein, we revisit the problem of predicting dopability of semiconductors and build upon these previous works. We ask the question of the complete set of governing intrinsic material properties and the causal relationship between them, without making the largely qualitative and heuristic assumptions about the alignment of the pinning energies or the connection of dopability to the branch point energy. We do this by formulating a model description of a binary ionic semiconductor using the tight-binding model for noninteracting electrons supplemented by the nucleus-nucleus repulsion (pair) potential. We use this model to derive analytic expressions for the formation energy of intrinsic donors and acceptors and the associated doping pinning energies. The model is validated against the directly calculated (firstprinciples) pinning energies. Finally, we analyze the new insights that are provided by the model, the role of previous heuristics, as well as its utility in searching for dopable materials. It is important to note, however, that modern defect theory and defect calculations on the used to predict both intrinsic limits to dopability (doping pinning energies) and the

effectiveness of extrinsic dopants.<sup>89,98</sup> The aim here is to uncover the physical principles of semiconductor dopability that are usually implicit and hidden in numerical approaches.

## DOPABILITY MODEL

**Construction.** Let us consider a binary  $C_1A_1$  ionic semiconductor defined as follows:

- (i) it is composed of two kinds of atoms A and C: one more electronegative taking the role of an anion (A) and the other less electronegative (cation-C),
- (ii) every anion (cation) contributes  $n_{\rm a}$  ( $n_{\rm c}$ ) number of atomic orbitals and  $N_{\rm a}$  ( $N_{\rm c}$ ) number of electrons where the charge balance between the cations and anions implies  $N_{\rm a}+N_{\rm c}=n_{\rm a}$ ,
- (iii) electrons interact only with the nuclei and not among themselves (independent electron approximation),
- (iv) band gap forms between two bands: the valence band that is predominantly of the anion character and the cation-derived conduction band (Figure 3, topmost panel),
- (v) defects such as anion or cation vacancies only affect the valence band (anion defects) or conduction band (cation defects) densities of states, while interstitial defects add atomic orbitals with the energy that falls in the middle of the corresponding band (Figure 3, lower panels), and
- (vi) we also neglect any changes to the density of states that are due to relaxations of atomic positions upon defect formation.

For the sake of simplicity, we have intentionally neglected the possibility of vacancy states occurring deep inside the band gap. This is not a big limitation as the deep donors are typically fully ionized close to the top valence band, as are deep acceptors close to the bottom of the conduction band. Under these circumstances, the above assumptions should still apply. To describe this (idealized) binary system, we will utilize a model Hamiltonian with electrons described within the tight-binding approximation and the repulsion between nuclei through the pair potential term. <sup>99</sup> For our discussion, it is more useful to write the total energy of the system

$$E_{\text{tot}} = \sum_{k} \varepsilon_{k} f(\varepsilon_{k}, T) + \frac{1}{2} \sum_{i,j} V_{ij}$$
(1)

where the summation in the first term goes over all occupied electronic states as determined by the Fermi–Dirac distribution function  $f(\varepsilon_k T)$ , and the second term is the nuclear repulsion term. Note that this expression is only valid if the electron–electron interactions are neglected.

**Defect Formation Energies.** As already discussed, the intrinsic aspects of semiconductor dopability can be formulated in terms of the energy to form intrinsic compensating defects that prevent (compensate) the introduction of free charge carriers of the desired type (n or p). The energy to form a single point defect is given as

$$\Delta E_{\rm D} = E_{\rm tot}^{\rm Defect} - E_{\rm tot}^{\rm Host} \pm \mu \tag{2}$$

where  $E_{\rm tot}^{\rm Defect}$  and  $E_{\rm tot}^{\rm Host}$  represent the energy of the system with and without the defect D, respectively, while  $\mu$  is the chemical potential of the respective chemical reservoirs with which the exchange of atoms occurs upon forming the defect. The plus

sign in  $\pm\mu$  corresponds to vacancies, while the minus sign is used in case of interstitials.

Cation Vacancy. Within the above model, the formation of a cation vacancy will result in (i) the absence of a nucleus at a particular cation site  $\alpha$ , (ii) the removal of the  $N_c$  number of electrons from the system, and (iii) the reduction of the density of states primarily in the conduction band in the amount equal to the number of states  $n_c$  that each cation contributes to the system. As illustrated in Figure 3, we will

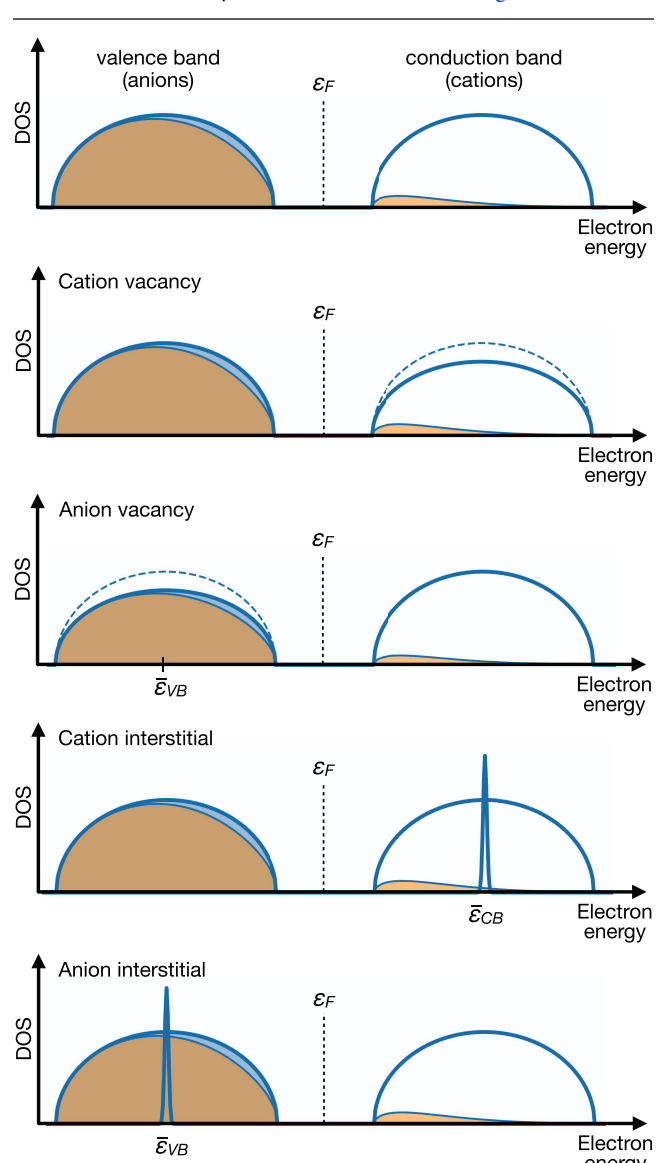


**Figure 3.** Schematics of the electronic density of states (DOS) assumed in our model (topmost panel), and the changes in the electronic DOS due to the formation of various types of vacancy and interstitial defects (lower panels). The shaded regions (in brown) in the figure represent the occupancy of the bands, based on the Fermi–Dirac statistics.

assume that this reduction in the number of conduction band states is distributed in a way that does not affect the average energy of conduction band, while the overall number of states is reduced by  $n_{\rm c}$ . It is also important to note that the Fermi statistics in combination with the largely unchanged DOS in the valence band implies that the  $N_{\rm c}$  number of holes created by removing one cation will thermalize over both valence and

conduction bands and will have the energy equal to the negative electron chemical potential or the Fermi energy ( $\varepsilon_{\rm F}$ ), as illustrated in Figure 3. By incorporating these considerations into eqs 1 and 2, the energy to form one cation vacancy ( $\Delta E_{V_c}$ ) becomes

$$\Delta E_{V_c} = -N_c \varepsilon_F - V_\alpha + \mu_c \tag{3}$$

where the first term on the right-hand side represents the energy contribution due to the difference in occupation of the electronic states between the defect and host systems ( $N_c$  holes with energy  $-\varepsilon_F$ ), the second  $V_\alpha = \sum_j V_{\alpha,j}$  term represents the energy difference in the nuclear repulsion due to the missing cation at the site  $\alpha$  (nuclear repulsion potential of that site), and, as before, the last term represents the cation chemical potential. In the derivation of eq 3, we also assumed that creating a cation vacancy does not appreciably affect the Fermi energy, i.e., the  $\varepsilon_F$  of the defect system equals that of the host. Rigorously, this assumption is valid in the case of low vacancy concentration (the dilute limit). Given the chemical composition and the crystal structure, which set the  $V_\alpha$  and some value of the cation chemical potential set by the state of the cation reservoir, the  $\Delta E_{V_c}$  becomes the decreasing function of the Fermi energy, as depicted in Figure 2.

of the Fermi energy, as depicted in Figure 2. As usually done in defect calculations,  $^{96,97}$  one can further separate the total chemical potential  $\mu_{\rm c}=\mu_{\rm c}^{\rm o}+\Delta\mu_{\rm c}$  into that of the standard cation phase at standard conditions  $(\mu_{\rm c}^{\rm o})$ , i.e., that of the solid metal at room temperature and ambient pressure, and the deviation from the reference value  $(\Delta\mu_{\rm c}<0)$ . Applying the same model Hamiltonian and the total energy formula from eq 1, one can write the reference chemical potential as  $\mu_{\rm c}^{\rm o}=N_{\rm c}\overline{\varepsilon}_{\rm c}+\overline{V}_{\rm c}$ , where  $\overline{\varepsilon}_{\rm c}$  represents a characteristic (average) energy of an electron in the reference phase, while  $V_{\rm c}$  stands for the average nuclear repulsion energy (per nucleus). While we keep  $\overline{\varepsilon}_{\rm c}$  as a separate entity, it is worthwhile noting that one can think of  $\overline{\varepsilon}_{\rm c}$  as approximately at the same energy as the center of the conduction band. After implementing these equations for the chemical potential, the formation energy of the cation vacancy becomes

$$\Delta E_{V_c} = N_c(\overline{\varepsilon}_c - \varepsilon_F) + (\overline{V}_c - V_\alpha) + \Delta \mu_c \tag{4}$$

This equation provides a relatively simple physical picture of the cation vacancy formation, which involves transfer of  $N_{\rm c}$  electrons from the system into the reference phase quantified by the energy of that transfer (first parentheses) and transfer of a cation nucleus from the system into the reference phase quantified by the difference in the nuclear repulsion (second parentheses). The last term describes the deviation of the actual cation reservoir from the standard state and is a function of the parameters such as temperature and pressure. Finally, it is important to note that  $\overline{\epsilon}_{\rm c}$  and  $\epsilon_{\rm F}$  need to be expressed relative to the common reference, which is usually assumed to be the vacuum level. Please note that Varley et al. 100 recently showed that for the tetrahedrally bonded semiconductors, the cation vacancy formation energy can be correlated to the branch point energy.

Anion Vacancy. Analogously, in our model, the creation of an anion vacancy will result in (i) the absence of a nucleus at a particular anion site (let us label it  $\alpha$  again), (ii) the removal of the  $N_a$  number of electrons from the system, and (iii) the reduction of the density of states primarily in the valence band, in the integral amount equal to the number of states  $n_a > N_a$  that each anion contributes to the system. One can derive an

equation for the formation energy of an anion vacancy similar to eq 4 with one key difference. Now, the reduction in the number of valence band states needs to be taken into account. The easiest way to see how to include the reduction in the valence band DOS is to assume a low temperature relative to the band gap so that all valence band states are approximately fully occupied. If this is the case, then the difference in the summation over all occupied states will amount to the number of states that are missing  $(n_a)$  times the average energy of the valence band states  $(\overline{\epsilon}_{VB})$ . Also, the  $N_c$  electrons that were previously occupying the missing states in the valence band will now be thermalized across the band gap giving rise to the  $N_c \varepsilon_F$  term. Taking all of these contributions into account, the anion vacancy formation energy is given as

$$\Delta E_{V_{a}} = N_{c} \varepsilon_{F} - n_{a} \overline{\varepsilon}_{VB} - V_{\alpha} + \mu_{a}$$
(5)

After applying the already described procedure for  $\mu_a$ , and noting that  $N_a + N_c = n_a$ , the anion vacancy formation energy becomes

$$\Delta E_{V_{a}} = N_{c}(\varepsilon_{F} - \overline{\varepsilon}_{VB}) + N_{a}(\overline{\varepsilon}_{a} - \overline{\varepsilon}_{VB}) + (\overline{V}_{a} - V_{a}) + \Delta \mu_{a}$$
(6)

where, as before,  $\overline{\varepsilon}_a$  represents some characteristic electronic energy of the anion reference phase (close to the center of the valence band), and  $\overline{V}_a$  stands for its average nuclear repulsion. Hence, the formation of an anion vacancy requires energy, which is an increasing function of  $\varepsilon_F$  and involves transfer of the cation electrons  $(N_c)$  from the valence band to the  $\varepsilon_F$ , transfer of the anion electrons  $(N_a)$  from the valence band into the anion reference phase, transfer of the anion nucleus from the system into the anion reference phase, and, as before, the last term describes the deviation of the actual anion reservoir from the standard state.

Interstitial Defects. To first order the interstitial defects, either the cation or the anion ones can be approximated as contributing their atomic orbitals and their valence electrons to the system. The cation interstitial will contribute the  $n_c$ number of localized states at approximately the midconduction band energy and the  $N_c$  number of electrons that would follow the Fermi-Dirac distribution and distribute themselves within the valence and the conduction bands so that their average energy in the dilute limit will become  $\varepsilon_{\rm E}$ , as illustrated in Figure 3. The anion interstitial, on the other hand, contributes  $n_a$  partially filled orbitals with  $N_a$  electrons at the mid-valence band. Because of the charge transfer to fill these states, there will be  $N_c = n_a - N_a$  holes created, having the energy  $\varepsilon_{\rm F}$ . The formation of these two defects requires the energy that can be derived in a similar fashion like that of the previous two amounting to

$$\begin{split} \Delta E_{I_{c}} &= N_{c}(\varepsilon_{F} - \overline{\varepsilon}_{c}) + (V_{\alpha} - \overline{V}_{c}) - \Delta \mu_{c} \\ \Delta E_{I_{a}} &= N_{a}(\overline{\varepsilon}_{VB} - \overline{\varepsilon}_{a}) + N_{c}(\overline{\varepsilon}_{VB} - \varepsilon_{F}) + (V_{\alpha} - \overline{V}_{a}) - \Delta \mu_{a} \end{split}$$

$$(7)$$

where  $\Delta E_{I_c}$  and  $\Delta E_{I_a}$  stand for the formation energy of the cation and anion interstitial defects, respectively, occupying lattice sites that are labeled  $\alpha$  in both cases.

**Dopability Metrics and the Emerging Design Principles.** The relevance of the previous derivations to the question of dopability, the very topic of this paper, follows from Zunger's formulation of dopability<sup>93</sup> in terms of the intrinsic compensating defects and the corresponding doping

pinning energies  $\varepsilon_{\rm F}^{(n)}$  and  $\varepsilon_{\rm F}^{(p)}$ , as already described (see Figure 2). The usual culprits preventing (compensating) the introduction of electrons into the conduction band are the intrinsic acceptor defects such as the cation vacancies and/or anion interstitials, while the anion vacancies and cation interstitials typically obstruct p-type doping. Having this in mind, the expressions for  $\varepsilon_{\rm F}^{(n)}$  and  $\varepsilon_{\rm F}^{(p)}$ , in Figure 2, can be defined as

$$\begin{split} \varepsilon_{\mathbf{F}}^{(\mathbf{n})} &= \min\{\varepsilon_{\mathbf{F}}^{(V_c)}, \, \varepsilon_{\mathbf{F}}^{(I_a)}, \, \ldots\}, \\ \varepsilon_{\mathbf{F}}^{(\mathbf{p})} &= \max\{\varepsilon_{\mathbf{F}}^{(V_a)}, \, \varepsilon_{\mathbf{F}}^{(I_c)}, \, \ldots\} \end{split} \tag{8}$$

where the n-type doping limit  $\varepsilon_F^{(n)}$  is the minimal doping pinning energy among all of the intrinsic acceptor defects, while the p-type doping limit  $\varepsilon_F^{(p)}$  is the maximal doping pinning energy among all of the intrinsic donors.

To simplify the discussion, we will focus on vacancies because in binary systems, they are most often the doping-limiting defects, and will discuss how the main results change in case interstitial defects are the limiting factor. Also, to make the expressions easier for discussion, we will express pinning energies relative to the corresponding band edge as  $\varepsilon_{\rm F}^{\rm (n)}={\rm CBM}+\delta\varepsilon_{\rm F}^{\rm (n)}$  and  $\varepsilon_{\rm F}^{\rm (p)}={\rm VBM}-\delta\varepsilon_{\rm F}^{\rm (p)}$ , as shown in Figure 2. Under the assumption that vacancies determine the dopability of materials,  $\delta\varepsilon_{\rm F}^{\rm (n)}$  and  $\delta\varepsilon_{\rm F}^{\rm (p)}$  can be derived from the condition that the formation energy of the corresponding defect equals zero at the pinning energies. From eqs 4 and 6, one finds

$$\begin{split} \delta \varepsilon_{\mathrm{F}}^{(\mathrm{n})} &= \overline{\varepsilon}_{\mathrm{c}} - \mathrm{CBM} + \frac{1}{N_{\mathrm{c}}} (\overline{V}_{\mathrm{c}} - V_{\alpha}) + \frac{1}{N_{\mathrm{c}}} \Delta \mu_{\mathrm{c}} \\ \delta \varepsilon_{\mathrm{F}}^{(\mathrm{p})} &= \mathrm{VBM} - \overline{\varepsilon}_{\mathrm{VB}} + \frac{N_{\mathrm{a}}}{N_{\mathrm{c}}} (\overline{\varepsilon}_{\mathrm{a}} - \overline{\varepsilon}_{\mathrm{VB}}) + \frac{1}{N_{\mathrm{c}}} (\overline{V}_{\mathrm{a}} - V_{\alpha}) \\ &+ \frac{1}{N_{\mathrm{c}}} \Delta \mu_{\mathrm{a}} \end{split}$$

Within this model, the  $\delta \varepsilon_{\rm F}^{\rm (n)}$  and  $\delta \varepsilon_{\rm F}^{\rm (p)}$  effectively become n-and p-dopability metrics. The condition for ambipolar dopability requires both pinning energies to be deep inside the corresponding band, which then translates into requiring both  $\delta \varepsilon_{\rm F}^{\rm (n)}$  and  $\delta \varepsilon_{\rm F}^{\rm (p)}$  to be positive and large. The following design principles emerge from these requirements.

Design Principles for n-Type Dopability Limited by the Cation Vacancies. First, the CBM of the material needs to be as low as possible, however, and not relative to some global reference such as the universal pinning energy or the branch point energy, but relative to the characteristic electronic energy of the cation reservoir so as to maximize the  $\overline{\varepsilon}_{\rm c}$  – CBM term. If one thinks of  $\overline{\epsilon}_c$  as close in energy to the center of the conduction band, then maximization of the first term implies large conduction bandwidth. Second, to make  $(\overline{V}_c - V_a)/N_c$ large and positive, the nuclear repulsion in the cation reservoir needs to be larger than that in the compound, and if this is the case, one wants  $N_c$  to be small (cation valency). Inversely, if  $\overline{V}_c$  $-V_{\alpha}$  < 0, the n-type dopability would require  $N_{c}$  to be large so as to minimize the harmful influence of this term. However, to accurately assess the influence of this term, one needs to know the actual pair potential for a particular system. We will return to this question later.

Design Principles for p-Type Dopability Limited by the Anion Vacancies. Maximization of the  $\delta \varepsilon_{\rm F}^{({\rm p})}$  implies qualitatively different requirements. Maximizing the first term

demands the VBM to be above the mean valence band energy  $(\overline{\epsilon}_{\rm VB})$ . This is always true, but this term is large only in systems with large valence bandwidths. Alternatively, one could imagine increasing VBM  $-\overline{\epsilon}_{\rm VB}$  by having additional valence bands located above the anion band. While not captured by the original model, this will be discussed later in the text. The second term is likely very small because, to first order, one can think that  $\overline{\epsilon}_a \approx \overline{\epsilon}_{\rm VB}$ . Much like before, one would like to have  $N_a/N_c$  large or small depending on the sign of the energy difference. The third term is analogous to the one for n-dopability and demands the nuclear repulsion to be higher in the anion reservoir than in the actual system weighed by the  $1/N_c$  term.

The meaning of the  $\Delta\mu$  is the same for both n- and pdopability. Since  $\Delta \mu \leq 0$ , it is desirable to have synthesis conditions to be as close to  $\Delta \mu = 0$  as possible. In other words, one wants to be as rich in the corresponding element as possible to prevent the formation of its vacancies. In binary systems,  $\Delta \mu = 0$  is typically a boundary of the stability region for both cations and anions. We will therefore assume in the remainder of this paper that  $\Delta \mu = 0$  condition can always be fulfilled. For the purpose of comparing the model with the explicit defect calculations, this is a fair assumption because  $\Delta \mu$ term is the same in both the cases and, hence, exactly cancels out. However, one needs to be cognizant of the fact that in chemical systems with many competing phases,  $\Delta \mu = 0$  might not be possible to achieve for all phases and for both cations and anions, and that the  $\Delta\mu$  term may appear as a limiting factor to dopability. However, even in such scenarios, the actual range of  $\Delta \mu$ , based on phase stability analysis, can be accommodated in the model, to provide reasonable estimates for  $\delta \varepsilon_{\rm F}^{\rm (n)}$  and  $\delta \varepsilon_{\rm F}^{\rm (p)}$ .

The design principles change in the case of interstitials. Similar analysis (see the Supporting Information for equations) shows that if the donor-behaving cation interstitial is the lowest-energy defect close to the VBM, then maximizing p-type dopability would require (i) that the VBM is as high as possible relative to the  $\overline{\varepsilon}_{\rm c}$  and (ii) that nuclear repulsion at the interstitial site  $V_{\alpha}$  is much larger than  $\overline{V}_{\rm c}$  together with the

Table 1. List and Description of Various Terms Appearing in Our Dopability Models Is Given Together with the List of Physical Quantities and/or Proxies Employed in the Model Validation

term	description	quantity or proxy used in validation (symbol)
$\overline{arepsilon}_{ m c}$	average electronic energy in the cation reference phase	work function of the cation reference phase $(W_c)$
$\overline{\mathcal{E}}_{\mathrm{a}}$	average electronic energy in the anion reference phase	work function of the anion reference phase $(W_a)$
$\overline{V}_{c} - V_{\alpha}$	difference in nuclear repulsion between the cation	compound's enthalpy of formation $(\Delta H_{ m f})$
	reference phase and site $\alpha$ in the compound	
$\overline{V}_{\rm a}-V_{lpha}$	difference in nuclear repulsion between the anion	compound's enthalpy of formation $(\Delta H_{ m f})$
	reference phase and site $\alpha$ in the compound	
$\overline{arepsilon}_{ ext{VB}}$	average energy of valence band states	calculated from the density of states
$\overline{\mathcal{E}}_{\mathrm{c}}^{\mathrm{s}}$	average energy of cation-s states	calculated from the density of states
CBM	conduction band minimum	GW calculated absolute CBM
VBM	valence band maximum	GW calculated absolute VBM $$

relatively small  $N_{\rm c}$  or in the case of  $V_{\alpha} < \overline{V}_{\rm c}$ , the  $N_{\rm c}$  needs to be large. In the case of the anion interstitials, the n-dopability would benefit from (i) small valence bandwidths and small band gaps, (ii) anions with low-lying atomic orbitals, and (iii) high nuclear repulsion on the interstitial site.

As evident from this discussion, the dopability of semiconductors does not depend on a single material property and is a product of relatively complex trade-offs between different properties. Also, as previously noted, the interstitial defects are usually higher in energy than vacancies in the simple binary systems considered here. This is particularly true for the anion interstitials due to their ionic sizes requiring a large amount of space. This is why in the remainder of the text, we will focus on vacancies as dominant dopability-limiting factors. Only one compound in our study, Mg<sub>2</sub>Si, turns out to have its p-type dopability limited by the cation (Mg) interstitials, for which we do consider the described interstitial defect model.

#### VALIDATION

Validation of our model is done by comparing how accurately it reproduces numerical values for the dopability metrics,  $\delta arepsilon_{
m F}^{
m (n)}$ and  $\delta \varepsilon_{\rm F}^{({\rm p})}$ , which we compute directly using modern defect theory and defect calculations. However, the quantities appearing in eq 9 are not easily accessible causing direct evaluation of the model dopability metrics difficult. This is particularly the case for the average electronic energies of the elemental reservoirs  $(\overline{\varepsilon}_c, \overline{\varepsilon}_a)$ , as well as the ionic repulsion terms (V) for both the elemental reservoirs and the material of interest. The approach we adopt here is to find proxies for these hard-to-access quantities instead of trying to calculate them directly. This approach follows the same idea as in our previous work in which we successfully developed models for electronic and heat transport in thermoelectric materials using more accessible proxies instead of hard-to-compute quantities. 91 If appropriate physical proxies can be found, a simplified model involving these proxies can be made computationally inexpensive, as well as predictive. The price of such an approach, however, is the introduction of free parameters into the model that need to be fit to the existing data. The performance of the model is then assessed by the quality of the fit. The following discussion focuses on the dopability metrics derived assuming vacancies as the lowest-energy compensating defects. Dopability metrics based on interstitial defects is also derived in the Supporting Information.

n-Type Dopability Metric. As shown in eq 9, there are three main contributions to  $\delta \varepsilon_{\rm F}^{\rm (n)}$ : the electronic term, nuclear repulsive term, and chemical potential term. The electronic term  $\overline{\varepsilon}_c$  – CBM involves the average electronic energy of the cation reference phase (solid metal) and the energy of the conduction band minimum. An intuitive proxy for  $\overline{\varepsilon}_c$ , which is easily accessible from the literature, is the negative work function  $(-W_c)$  of the reference phase. However, the work function of metals if expressed as an energy relative to vacuum (negative value) represents the maximal electronic energy and not an average one. Therefore, to account for the difference between  $\overline{\varepsilon}_c$  and work function, we consider replacing the first term with the proxy of the form  $a \times (-W_c) - b \times CBM$ , where a and b are the fitting constants,  $W_c$  is the work function of the metal phase, and CBM is the conduction band minimum (negative electron affinity) of the semiconductor material (measured or calculated). Both  $W_c$  and CBM are expressed relative to the vacuum.

To account for the nuclear repulsion contribution, one could fit the parameters of our tight-binding and nuclear repulsion Hamiltonian to a set of material properties such as the equilibrium volume, cohesive energy, bulk modulus, etc. While this would be the most appropriate thing to do, it would need to be done for all materials of interest and all elemental phases, which would render the whole process impractical. Among material properties, cohesive energies, volume, and bulk modulus are well known to be correlated with each other. 101,102 Hence, simply considering cohesive energy as a proxy for the nuclear repulsion contribution for a material could suffice. However, as we are interested in the difference  $(\overline{V}_c - V_a)$  between the compounds and the elemental phase energies, we chose  $\Delta H_f$  as a proxy as it already includes the difference between the compounds and the elemental phase energies and replaces the nuclear repulsion term with a linear dependence on the compound enthalpy of formation  $c \times \Delta H_f$ + d. Admittedly,  $\Delta H_f$  includes contributions from both electrons and nuclei. The choice is motivated by the physical relation to the nuclear repulsion and, in part, by our previous work in which we discovered the relevance of  $\Delta H_{\mathrm{f}}$  to the formation energy of oxygen vacancies in metal oxides. 103 The n-type dopability is evaluated under cation-rich condition such that  $\Delta\mu_{\rm c}$  = 0, because it represents the most favorable thermodynamic condition to dope the semiconductor n-type.

Finally, to extend the model to systems with partially oxidized cations such as the group-IV and group-V chalcogenides such as SnO, SnS, PbSe, PbTe, Bi<sub>2</sub>Se<sub>3</sub>, and Bi<sub>2</sub>Te<sub>3</sub>, one needs to include an additional term to account for the filled cation-s states that contribute to the valence band, as shown in Figure 4. This is easily done by including the transfer

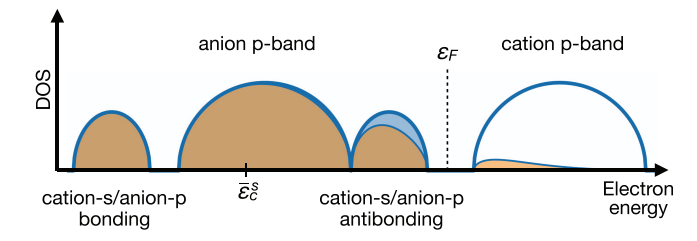


Figure 4. Schematic of the electronic DOS of binary systems with low valent cations such as the group-IV and group-V chalcogenides (SnO, SnS, PbSe, PbTe, Bi<sub>2</sub>Se<sub>3</sub>, and Bi<sub>2</sub>Te<sub>3</sub>). The "center of mass" of the filled cation-s contributions to the DOS is denoted as  $\overline{\mathcal{E}}_s^s$ .

of  $N_c^s$  number of the cation-s electrons from the valence band to the cation reservoir upon forming the cation vacancy. This term can be written as  $N_c^s(\overline{\varepsilon}_c - \overline{\varepsilon}_c^s)$ , where  $\overline{\varepsilon}_c$  is the average electronic energy of the cation reference phase, while  $\overline{\varepsilon}_c^s$  is the average energy of the cation-s states in the material's valence band (s-DOS center of mass). The latter is obtained from the bulk electronic structure calculations, similar to the average energy of the anion-p states in the p-type dopability metric. The n-dopability metric, formulated in terms of the proxies, is now given as

$$\delta \varepsilon_{\rm F}^{\rm (n)} = a^{\rm (n)} \times W_{\rm c} - b^{\rm (n)} \times {\rm CBM} - c^{\rm (n)} \times \overline{\varepsilon}_{\rm c}^{\rm s} + d^{\rm (n)} \times \Delta H_{\rm f} + e^{\rm (n)}$$
(10)

where  $a^{(n)}$ ,  $b^{(n)}$ ,  $c^{(n)}$ ,  $d^{(n)}$ , and  $e^{(n)}$  are the free parameters of the model (fitting constants), which are obtained by fitting to the directly calculated  $\delta \varepsilon_{\rm F}^{(n)}$  from first-principles defect calculations. The above form also allows extending the model to any  ${\rm C}_x{\rm A}_y$ 

stoichiometry (not only  $C_1A_1$ ). The list of terms appearing in the models, as well as the corresponding proxies we use for validation, is given in Table 1

**p-Type Dopability Metric.** Analogously, terms such as VBM,  $\overline{\varepsilon}_{\rm a}$ , and  $(\overline{V}_{\rm a}-V_{\alpha})$  in the definition of  $\delta\varepsilon_{\rm F}^{(\rm p)}$  are substituted with the valence band maximum (negative ionization potential) of the semiconductor, negative work function of the anion reference phase or in the case of molecules, negative first ionization potential  $(-W_{\rm a})$ , and the compound's enthalpy of formation. As discussed earlier, the ptype dopability metric has an additional term  $(\overline{\varepsilon}_{\rm VB})$  representing the average energy of the valence band, which we evaluate for a set of classic binary semiconductors as the average energy of the anion-p states. This is done from the electronic structure calculations (see the Methods section) of the bulk, defect-free materials. Finally, the p-type dopability is evaluated under anion-rich conditions such that  $\Delta\mu_{\rm a}=0$ . The p-dopability metric, formulated in terms of proxies, is given as

$$\delta \varepsilon_{\rm F}^{(\rm p)} = a^{(\rm p)} \times W_{\rm a} + b^{(\rm p)} \times {\rm VBM} - c^{(\rm p)} \times \overline{\varepsilon}_{\rm VB} + d^{(\rm p)} \times \Delta H_{\rm f} + e^{(\rm p)}$$
(11)

where, as before,  $a^{(p)}$ ,  $b^{(p)}$ ,  $c^{(p)}$ ,  $d^{(p)}$ , and  $e^{(p)}$  are the free parameters that are fitted to the directly calculated  $\delta \varepsilon_{\rm F}^{(p)}$ . For each  $\delta \varepsilon_{\rm F}^{(n)}$  and  $\delta \varepsilon_{\rm F}^{(p)}$ , we have a total of five fitting constants, which we fit to a set of 16 materials as described further.

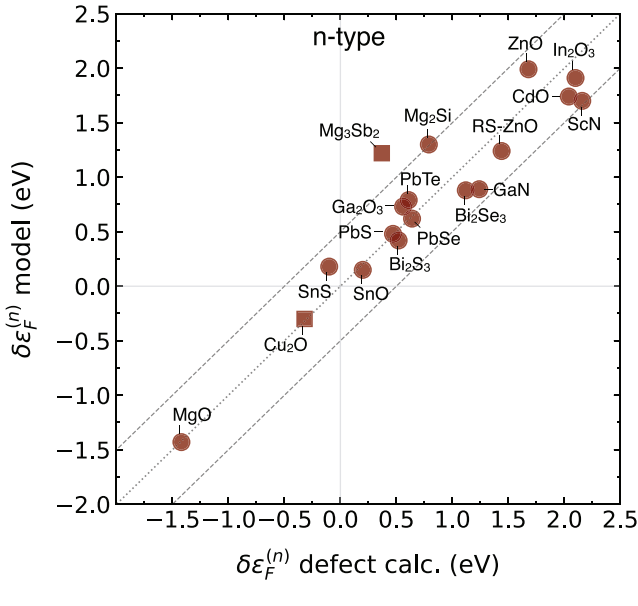
The work functions for the cation reference phases, the ionization energies for the gaseous species such as O<sub>2</sub> and N<sub>2</sub>, and the enthalpy of formations are obtained from refs 104 and 105, with details provided in Table S5 of the Supporting Information (SI). Compounds' conduction band minima and valence band maxima (with respect to vacuum) are explicitly calculated using the standard methodology, involving the combination of *GW* electronic structure and density functional theory (DFT) surface calculations. Experimental CBM and VBM values are used for Ga<sub>2</sub>O<sub>3</sub> and In<sub>2</sub>O<sub>3</sub>. Details of all of the above intrinsic material properties of the compounds, along with the average energy of the anion-p and cation-s states (obtained from calculated DOS) employed in our model, are provided in Table S6 of the SI.

We performed defect calculations for a set of 16 binary ionic semiconductors, including classic III—Vs and II—VIs, group-III oxides, and lead and bismuth chalcogenides. Results of the fitting of the n and p-type dopability metrics (eqs 10 and 11) to the same quantities from defect calculations are shown in Fig 5. We use the standard linear regression to obtain values for the fitting parameters. The quality of the fit (as shown in Figure 5) is very good with the  $R^2 = 0.91$  and 0.81 and rootmean-square error (RMSE) = 0.26 and 0.25 eV for n and p-type dopability metrics, respectively. The final expressions for the two dopability metrics are

$$\delta \varepsilon_{\rm F}^{\rm (n)} = 1.40 W_{\rm c} - 0.60 \text{CBM} + 0.05 \overline{\varepsilon}_{\rm c}^{\rm s} + 0.03 \Delta H_{\rm f} + 4.79$$

$$\delta \varepsilon_{\rm F}^{\rm (p)} = 0.09 W_{\rm a} - 0.03 \text{VBM} + 0.37 \overline{\varepsilon}_{\rm VB} - 0.12 \Delta H_{\rm f} + 2.81$$
(12)

In addition to relying only on the quality of the fit, our model from eq 12 was further validated against three additional compounds,  $Mg_3Sb_2$ , KSb, and  $Cu_2O$ , that were not included in the fitting. As shown in Figure 5, both p- and n-type dopability fit very well for  $Mg_3Sb_2$  because the bonding in  $Mg_3Sb_2$  satisfies the model assumptions. The p-type dopability in KSb fairs well because the valence band is composed of



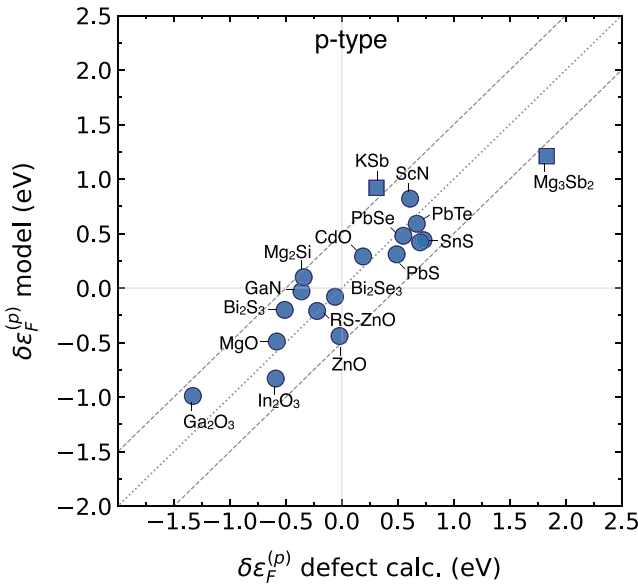


Figure 5. Comparison of the analytic model and the calculated (from first-principles defect calculations) n- and p-type dopability metrics  $\delta \varepsilon_F^{(n)}$  and  $\delta \varepsilon_F^{(p)}$ . The model parameters from eqs 10 and 11 are obtained via linear regression to the calculated values. Mg<sub>3</sub>Sb<sub>2</sub>, KSb, and Cu<sub>2</sub>O (shown as squares) are employed for model validation and are not included in the fitting. See the text for more details.

anion (Sb)-p states. However, the n-type dopability for KSb does not agree with the model (not shown), which is not surprising, because the conduction band of KSb does not follow the assumptions of the model, i.e., it is composed of the Sb-p orbitals. The original model also does not capture many transition metal compounds that often have contributions of the metal-d states to both valence and conduction bands. However, for systems such as  $\text{Cu}_2\text{O}$  where the conduction band is largely composed of Cu-s states, our model still works well for the n-type dopability, as illustrated in Figure 5. The p-type dopability is not well captured because Cu-d states contribute heavily to the valence band but not to the conduction band. That said, the model itself can be modified to include these various cases.

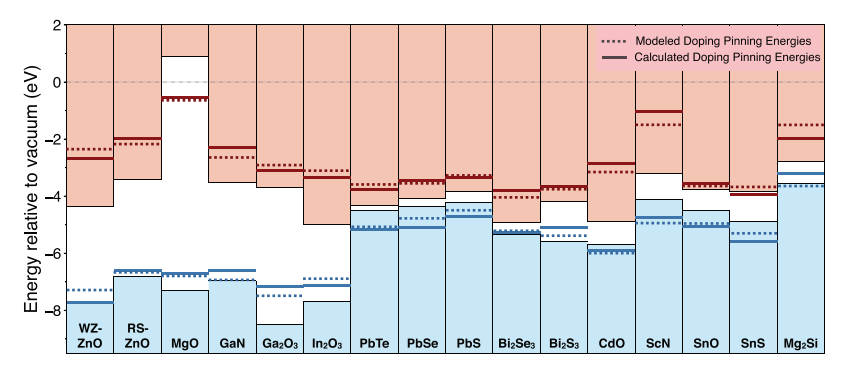


Figure 6. Doping pinning energies both from direct defect calculations (solid lines) and from our models (dashed lines) are shown together with the absolute band edge position (colored rectangles) for all 16 materials considered in this work.

It is important to note that all of the modeled values of  $\delta \varepsilon_{\rm F}^{({\rm n})}$ and  $\delta \varepsilon_{\rm F}^{(\rm p)}$  are within 0.5 eV compared to the values from the defect calculations, which is, in our opinion, striking given the simplifications and approximations adopted in the model. The magnitude of the coefficients and the contribution of each term in eq 12 vary with the dopability type. For the n-type pinning energy,  $\delta \varepsilon_{\rm F}^{\rm (n)}$ , individual terms comprising  $W_{\rm c}$ , CBM, and the intercept term contribute more significantly because they are about an order of magnitude larger than the terms comprising  $\overline{\mathcal{E}}_{\mathrm{c}}^{\mathrm{s}}$  and  $\Delta H_{\mathrm{f}}$  However, for the p-type pinning energy,  $\delta \mathcal{E}_{\mathrm{f}}^{(\mathrm{p})}$ , individual terms comprising  $\overline{\epsilon}_{VB}$  and the intercept have an order of magnitude larger coefficients than the  $W_a$ , VBM, and  $\Delta H_{\rm f}$  terms. We will return to the question of dominant terms in the Discussion section. It is also important to note that some of the coefficients turn out to be negative. This is possible because (i) when substituting physical quantities for proxies, we do not know the actual dependencies between the two, (ii) by using the work functions, we are using the maximal electronic energy of the elemental reservoirs rather than the average one, and, finally, (iii) we are folding both the dependence on the actual stoichiometry and the number of valence electrons of cations and anions into the fitting coefficients, which could also alter the signs of the coefficients. By doing so, we are trying to develop a model that is simple to use. Obviously, the choices we made are not unique, and one could in principle come up with a different set of proxies and a different numerical model.

# DISCUSSION

The dopability metrics  $\delta \varepsilon_{\rm F}^{\rm (n)}$  and  $\delta \varepsilon_{\rm F}^{\rm (p)}$  and the resulting doping pinning energies are shown in Figure 6 alongside the absolute band edge positions for all 16 materials considered in this study. All energies are shown relative to the vacuum level. The  $\varepsilon_{\rm F}^{\rm (n)}$  and  $\varepsilon_{\rm F}^{\rm (p)}$  from defect calculations are represented as continuous lines, while those resulting from the model, eq 12, are depicted as dashed lines. The position of the pinning energies relative to the band edges determines the dopability of a material. For example, if the pinning energies  $arepsilon_{
m F}^{({
m n})}$  and  $arepsilon_{
m F}^{({
m p})}$  are both inside the corresponding bands (meaning  $\delta \varepsilon_{\rm F}^{\rm (n)} > 0$  and  $\delta \varepsilon_{\rm F}^{(\rm p)} > 0$ ), the compound allows both p- and n-type doping, likely to the degenerate levels. Conversely, if one of the doping pinning energies is inside the band gap, the dopability of the material to the corresponding carrier type is reduced and even diminished depending on the distance from the band edge. If both doping pinning energies are deep inside the band gap, the material cannot be doped.

As evident from Figure 6, as well as from the previous discussion, there is a good overall correspondence between the calculated and modeled pinning energies. However, contrary to Zunger's finding for III—V and II—VI semiconductors, the doping pinning energies generally do not align. It is clear that if compounds outside these two groups are considered, the deviations in the positions of the doping pinning levels are significant (>2 eV). Hence, one cannot rely on the alignment of the pinning levels and a simple doping principle based on the band edges alone.

A lot of emphasis has been given previously to the absolute position of the band edges as a guiding principle. In addition to the work of Zunger and co-workers, <sup>93,107</sup> Walukiewicz<sup>108</sup> and Schleife et al. <sup>94</sup> discussed how the band edge energies, expressed relative to a universal branch point energy, correlate with dopability. In all of these works, it was found that the n-type dopable materials typically have high electron affinity (low CBM), while the p-dopable materials have small ionization potentials (high VBM). <sup>94,109</sup>

Absolute VBM and CBM also appear in our model as properties influencing material dopability. Our derivation explains why they correlate with dopability, but also reveals that these are not the only relevant properties as one can clearly see that the dopability trends do not exactly correspond to the trends in the band edge positions. For example, GaN, Ga<sub>2</sub>O<sub>3</sub>, and In<sub>2</sub>O<sub>3</sub> are all degenerately n-dopable despite large differences in their CBM positions. Also, SnO and SnS are only moderately n-dopable while having their CBMs below GaN, etc. An obvious question that follows from this discussion is whether a model of dopability that includes only the band edges can be constructed?

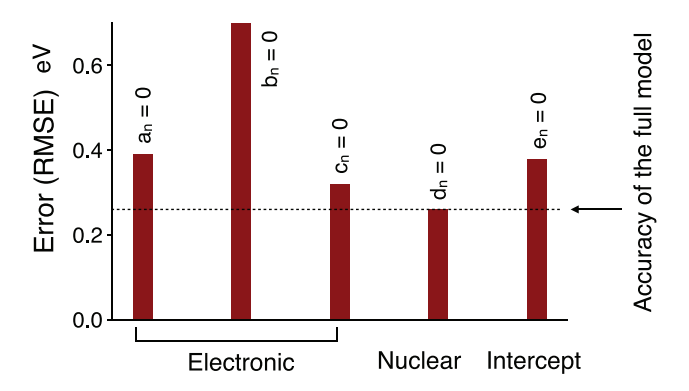
**Description from the Band Edges Alone.** To answer this, we repeated the fitting exercise from the Validation section by only including the absolute band edge terms and the free parameter (intercept). The simplified dopability metrics are then given as  $\delta e_{\rm F}^{(n)} = -b^{(n)} \times {\rm CBM} + e^{(n)}$  and  $\delta e_{\rm F}^{(p)} = b^{(p)} \times {\rm VBM} + e^{(p)}$ . The fit thus performed resulted in the root-mean-square errors (RMSEs) of 0.67 and 0.41 eV for the n- and p-type dopability, respectively, compared to the RMSEs of 0.26 eV (n-type) and 0.25 eV (p-type) for the full model. So, using only the band edge positions as descriptors of dopability is much less accurate than the full model.

Including the work functions to the two metrics,  $\delta \varepsilon_{\rm F}^{\rm (n)} = a^{\rm (n)} \times W_{\rm c} - b^{\rm (n)} \times {\rm CBM} + e^{\rm (n)}$  and  $\delta \varepsilon_{\rm F}^{\rm (p)} = a^{\rm (p)} \times W_{\rm a} + b^{\rm (p)} \times {\rm VBM} + e^{\rm (p)}$ , helps improve the model significantly to RMSEs of 0.34 (n-type) and 0.31 (p-type). This further supports one of the key implications of our model. It is not the absolute VBM and CBM that matter but the VBM and CBM relative to the

average electronic energies of the elements, which are, in this case, represented by their work functions. That said, the absolute VBM and CBM could serve as coarse guidelines but one needs to be aware that the error in the doping pinning energies can likely be much above 0.5 eV.

Furthermore, to gauge the importance of each individual term, we performed an exercise of removing terms one at a time (by putting their coefficient to zero) and re-doing the fit. As discussed previously, these terms can be grouped into electronic contributions, comprising reference phase work function  $(a \times W)$ , absolute band edge positions  $(b \times \text{CBM})$  or VBM), average electronic energy of cation-s  $(c \times \overline{e}_c^s)$  or valence band states  $(c \times \overline{e}_{VB})$  and nuclear repulsion  $(d \times \Delta H_f)$ , and a free parameter (intercept term e). Based on the results (RMSE values) summarized in Figure 7, we can draw the following

$$\delta \epsilon_F^{(n)} = a_n x W_c - b_n x CBM - c_n x \epsilon_c^s + d_n x \Delta H_f + e_n$$



$$\delta \epsilon_F^{(p)} = a_p \times W_a + b_p \times VBM - c_p \times \epsilon_{vb} + d_p \times \Delta H_f + e_p$$

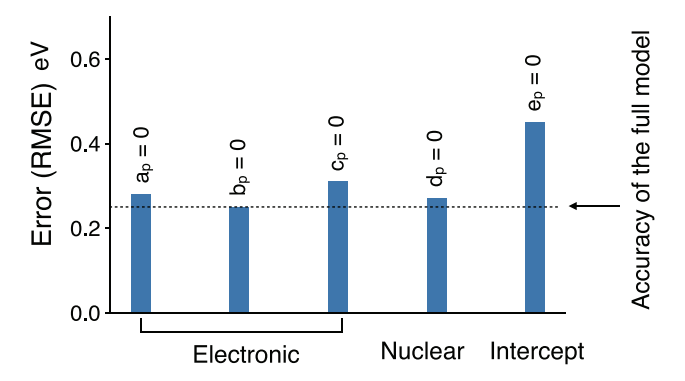


Figure 7. Comparing the error in the modeled pinning energies when individual terms in eqs 10 and 11 are removed one at a time (by setting the respective coefficients to zero) vs the full model.

conclusions: (1) n-type doping metric  $\delta \varepsilon_{\rm F}^{\rm (n)}$  depends more significantly on the electronic contributions than the p-type doping metric  $\delta \varepsilon_{\rm F}^{\rm (p)}$ , (2) within the electronic terms, both the reference phase work function and the compounds' CBM are needed to accurately reproduce both  $\delta \varepsilon_{\rm F}^{\rm (n)}$  and  $\delta \varepsilon_{\rm F}^{\rm (p)}$ , and, finally, (3) the intercept is important, especially in the case of  $\delta \varepsilon_{\rm F}^{\rm (p)}$ . Please note that the intercept integrates both electronic and nuclear contributions that are not easily separated.

Role of the Band Gap. Magnitude of the electronic band gap is another quantity used to gauge the dopability of semiconductors. It follows from the observation that the wider the gap is, the more insulating or less dopable a material is likely to be. While generally true, this coarse rule of thumb

does not provide any insight into the apparent doping asymmetry (typically toward the n-type) of many semiconductors. Also, there are exceptions from this rule like MgO, for example. MgO is a large band gap (~7.7 eV) material and is moderately p-type dopable, 110 which is in agreement with the predicted p-doping pinning energy that appears near the VBM in Figure 6. Our approach shows that the band gap of the material does not appear to be a governing factor in determining dopability. What matters are the positions of individual band edges, the characteristic electronic energy of the corresponding reference phase, average band energies, bandwidths, and nuclear repulsions due to creation of a defect.

The only place where the band gap explicitly appears is in the n-type dopability when limited by the anion interstitials (see the Dopability Metrics and the Emerging Design Principles section). One of the conditions demands that the difference between the center of the valence band and the conduction band minimum  $\overline{\varepsilon}_{VB}$  – CBM be as large as possible. Since  $\overline{\varepsilon}_{VB}$  < CBM, the only way to accomplish this is to have CBM to be as close to  $\overline{\varepsilon}_{VB}$ , which implies having narrow valence bandwidth and small band gap, both at the same time. However, since the anion interstitials are rarely low-energy defects in binary systems, the explicit role of the band gap is not very prominent.

However, the likelihood for the conditions for the vacancy-limited p- and n-type dopability to be simultaneously fulfilled is higher in low gap systems, although not exclusively. Recall that the approximate way to treat the average electronic energies of the reference phases is to assume that they are close to the conduction and valence band centers. Then, the ambipolar dopability demands large bandwidths for both valence and conduction bands. This is more often the case in narrow-gap systems than in wide-gap systems, although one cannot neglect exceptions to this relatively naive expectation. There is nothing that in principle forbids moderate- to wide-gap systems to have large bandwidths and there are also trade-offs with other properties that could make up for the bands that are not as wide.

Extrinsic Defects, Covalent and Multinary Systems, and the Utility in Material Searches. Dopability of a semiconductor can also depend on the availability of an appropriate external dopant. The dopant's effectiveness, in addition to the host material not developing intrinsic compensating defects (the subject of this paper), will depend on (1) its solubility in the host material and (2) its preference toward the expected behavior (donation or acceptance of charges). For example, as Figure 6 suggests, ZnO in its groundstate wurtzite structure should be moderately p-type dopable. Not to degenerate levels, but nevertheless it should be possible to dope it p-type. Based on the solubility among the external dopants, Li (group-I) and N (group-V) are best suited for this purpose. However, Li fails to dope ZnO p-type because it is present in nearly equal amount both as a substitutional acceptor  $(Li_{7n}^{1-})$  and as interstitial donor  $(Li_{1}^{1+})$ . Hence, it almost self-compensates resulting in a very low net hole concentrations. N, on the other hand, acts as a deep acceptor in ZnO and needs high ionization energy to provide any measurable free carriers at room temperature. In ZnO, the ptype doping is also made difficult because of the presence of hydrogen (acting as a donor) as an unintentional contaminant during growth techniques. 26,82,111

In principle, our model can be extended to include extrinsic defects. This would require knowledge of the position of the atomic orbitals of extrinsic dopants relative to the band edges of the host, as well as assumptions (or a model) pertaining to the defect states within the host. Also, the present model is developed for ionic and partially ionic semiconductors. Therefore, it is not expected to apply to fully covalent systems such as the elemental Si, Ge, diamond, and others. In these cases, defects such as vacancies introduce states deep inside the band gap, in addition to renormalizing the valence and conduction band density of states. Such deep defect states can both accept and donate charges and, hence, can limit both the p- and n-type doping. While the model can be extended to cover fully covalent materials, in this paper, we have focused on ionic or partially ionic semiconductors as they constitute a larger group of materials.

The model description would also become much more complex if one moves beyond the elemental and binary semiconductors. In ternary and multinary systems, generally more than one atomic species contributes to the band edges, and therefore, it is likely that more than one model is required to cover different possible situations. Alternatively, for specific families among multinary compounds, such as Zintl phases, for example, one could try finding some other higher-level descriptors that could be helpful in large-scale material searches. 112

Finally, in regard to the large-scale material screening for dopability, the model we have developed could be useful, especially the version involving proxies from the Validation section, provided that a rapid evaluation of the absolute (or relative) VBM, CBM, and elemental work functions can be made possible. While the band edges are not the only governing properties, their contributions to the dopability of semiconductors cannot be ignored, not even approximately. The computational procedure to evaluate absolute VBM and CBM is nowadays well established; it includes the electronic structure calculations for the bulk in combination with the calculations of the surface dipoles. The surface calculations represent a real bottleneck to high-throughput screening as they are of the similar level of complexity as the direct defect calculations. So, until a more efficient way to evaluate absolute VBM and CBM positions is developed, relatively tedious and laborious direct defect calculations remain the only available choice for a robust prediction of the doping tendencies of materials.

# CONCLUSIONS

In conclusion, to reveal the intrinsic material properties that determine the dopability of semiconductors, we have developed a model description of the defect formation energies in ionic and partially ionic systems. The model is constructed using the tight-binding description of the electronic structure augmented by the nuclear repulsion (pair) potential term. Utilizing such an approach in combination with the existing formulation of the dopability in terms of the limiting (compensating) intrinsic point defects, we are able to analytically separate various contributions. Contrary to the presently adopted and largely heuristic view, the position of the band edges alone cannot be used to accurately describe the doping limits of semiconductors. In addition, the electronic structure of the elemental reservoirs has to be taken into account, as well as the differences in the nuclear repulsion between the material of interest and the elemental reservoirs.

Hence, the dopability of semiconductors is a result of a relatively complex trade-offs between various intrinsic properties. To make the model practical, as well as for the purpose of validation, we replace the hard-to-calculate quantities in the model with the more accessible ones and showed that the model is able to accurately reproduce the directly calculated (from modern defect calculations) doping limits of 16 classic binary semiconductors. Finally, we discuss the extension of our work to more complex chemistries and the utility in large-scale material searches.

#### METHODS

**First-Principles Defect Calculations.** In this work, we employ the standard supercell approach<sup>97</sup> using our computational framework<sup>113</sup> to calculate formation energies of point defects using the following equation

$$\Delta H_{D,q}(E_{F}, \mu) = [E_{D,q} - E_{H}] + \sum_{i} n_{i}\mu_{i} + qE_{F} + E_{corr}$$
(13)

where  $\Delta H_{\mathrm{D},q}$  represents the formation energy of a point defect D in charge state  $q_i$   $E_{\mathrm{D},q}$  and  $E_{\mathrm{H}}$  are the total energies of the supercells with and without the defect, respectively;  $\mu_i$  is the chemical potential of atomic species, i, describing the exchange of particles with the respective reservoirs;  $E_{\mathrm{F}}$  is the Fermi energy and is used here to account for the possible exchange of charge between the defect and the Fermi energy (i.e., the charge reservoir); and  $E_{\mathrm{corr}}$  is a correction term to account for the finite-size corrections within the supercell approach. The chemical potential  $\mu_i = \mu_i^0 + \Delta \mu_i$  is expressed relative to the reference elemental chemical potential  $\mu_i^0$ , calculated using the FERE approach (re-fitted for HSE calculations), and  $\Delta \mu_i$  is the deviation from the reference elemental phase, the bounds of which are determined by the thermodynamic phase stability.

A plane-wave energy cutoff of 340 eV and a Monkhorst-Pack kpoint sampling 115 are used. The low-frequency total (electronic + ionic) dielectric constant is obtained following the procedure in ref 116. We have implemented tools in our framework 113 to calculate the following finite-size corrections: (1) potential alignment, (2) imagecharge correction, and (3) band-filling correction to address Moss-Burstein-type effects. Beyond the finite-size effects, another source of inaccuracy arises from the well-known DFT band-gap problem. Accurate band gaps are needed to correctly describe the formation energy of charged defects as a function of the electronic chemical potential i.e., Fermi energy. We employ state-of-the-art *GW* quasi-particle energy calculations <sup>117</sup> to compute band edge shifts (relative to the DFT-computed band edges). The band edge shifts are used to correct the defect formation energy in multiply charged states. GW calculations are performed on the DFT-relaxed structures, with the unit cell vectors re-scaled to match the experimental lattice volume. <sup>116</sup> For hybrid functional (HSE06<sup>118,119</sup>) calculations, the exchange mixing is used accordingly to match their experimental lattice parameters and band gaps. Having defect formation energy allows thermodynamic modeling of defect and carrier concentrations, computed here using the approach from refs 36, 87, and 120. Confidence in our predictions stems from the correct description of defects and doping in our previous works, 36,87,113 demonstrating a good agreement between the calculated and measured defect and charge carrier concentrations in PbTe and other systems.

# ASSOCIATED CONTENT

#### **Solution** Supporting Information

The Supporting Information is available free of charge at https://pubs.acs.org/doi/10.1021/acs.chemmater.9b05126.

Additional details that may be necessary to validate our results and discussion presented in the main manuscript (PDF)

Detailed tabulated data of defect formation energies and converged calculation parameters (ZIP)

#### AUTHOR INFORMATION

# **Corresponding Author**

Vladan Stevanović – Colorado School of Mines, Golden, Colorado 80401, United States; Email: vstevano@mines.edu

#### **Authors**

- Anuj Goyal Colorado School of Mines, Golden, Colorado 80401, United States; oorcid.org/0000-0001-5991-9562
- Prashun Gorai Colorado School of Mines, Golden, Colorado 80401, United States; ⊙ orcid.org/0000-0001-7866-0672
- Shashwat Anand Northwestern University, Evanston, Illinois 60208, United States
- Eric S. Toberer Colorado School of Mines, Golden, Colorado 80401, United States
- G. Jeffrey Snyder Northwestern University, Evanston, Illinois 60208, United States

Complete contact information is available at: https://pubs.acs.org/10.1021/acs.chemmater.9b05126

#### **Notes**

The authors declare no competing financial interest.

#### ACKNOWLEDGMENTS

The authors thank Dr. Stephan Lany from National Renewable Energy Laboratory (NREL) for fruitful discussions. The authors acknowledge support from the NSF DMR program, grant nos. 1729594 and 1729487. This research used computational resources sponsored by the DOE Office of Energy Efficiency and Renewable Energy and located at the National Renewable Energy Laboratory. High-performance computational resources at the Colorado School of Mines are also acknowledged.

## REFERENCES

- (1) Williamson, B. A. D.; Buckeridge, J.; Brown, J.; Ansbro, S.; Palgrave, R. G.; Scanlon, D. O. Engineering Valence Band Dispersion for High Mobility p-Type Semiconductors. *Chem. Mater.* **2017**, 29, 2402–2413.
- (2) Varley, J. B.; Miglio, A.; Ha, V.-A.; van Setten, M. J.; Rignanese, G.-M.; Hautier, G. High-Throughput Design of Non-oxide p-Type Transparent Conducting Materials: Data Mining, Search Strategy, and Identification of Boron Phosphide. *Chem. Mater.* **2017**, *29*, 2568–2573
- (3) Varley, J. B.; Lordi, V.; Miglio, A.; Hautier, G. Electronic structure and defect properties of B<sub>6</sub>O from hybrid functional and many-body perturbation theory calculations: A possible ambipolar transparent conductor. *Phys. Rev. B* **2014**, *90*, No. 045205.
- (4) Burbano, M.; Scanlon, D. O.; Watson, G. W. Sources of Conductivity and Doping Limits in CdO from Hybrid Density Functional Theory. *J. Am. Chem. Soc.* **2011**, *133*, 15065–15072.
- (5) Sachet, E.; Shelton, C. T.; Harris, J. S.; Gaddy, B. E.; Irving, D. L.; Curtarolo, S.; Donovan, B. F.; Hopkins, P. E.; Sharma, P. A.; Sharma, A. L.; Ihlefeld, J.; Franzen, S.; Maria, J.-P. Dysprosium-doped cadmium oxide as a gateway material for mid-infrared plasmonics. *Nat. Mater.* 2015, 14, 414–420.
- (6) Dou, Y.; Egdell, R.; Walker, T.; Law, D.; Beamson, G. N-type doping in CdO ceramics: a study by EELS and photoemission spectroscopy. *Surf. Sci.* **1998**, *398*, 241–258.
- (7) Miller, S. A.; Dylla, M.; Anand, S.; Gordiz, K.; Snyder, G. J.; Toberer, E. S. Empirical modeling of dopability in diamond-like semiconductors. *npj Comput. Mater.* **2018**, *4*, No. 71.

- (8) Martinez, A. D.; Fioretti, A. N.; Toberer, E. S.; Tamboli, A. C. Synthesis, structure, and optoelectronic properties of  $II-IV-V_2$  materials. *J. Mater. Chem. A* **2017**, *5*, 11418–11435.
- (9) Biswas, K.; Zhao, L.-D.; Kanatzidis, M. G. Tellurium-Free Thermoelectric: The Anisotropic n-Type Semiconductor  $Bi_2S_3$ . *Adv. Energy Mater.* **2012**, *2*, 634–638.
- (10) Yu, D. n-Type Conducting CdSe Nanocrystal Solids. Science 2003, 300, 1277-1280.
- (11) Kumar, M.; Zhao, H.; Persson, C. Study of band-structure, optical properties and native defects in A I B III O<sub>2</sub> (A I = Cu or Ag, B III = Al, Ga or In) delafossites. *Semicond. Sci. Technol.* **2013**, 28, No. 065003.
- (12) Ibuki, S.; Yanagi, H.; Ueda, K.; Kawazoe, H.; Hosono, H. Preparation of n-type conductive transparent thin films of  $AgInO_2$ :Sn with delafossite-type structure by pulsed laser deposition. *J. Appl. Phys.* **2000**, *88*, 3067–3069.
- (13) Kumaravel, R.; Ramamurthi, K. Structural, optical and electrical properties of In-doped Cd<sub>2</sub>SnO<sub>4</sub> thin films by spray pyrolysis method. *J. Alloys Compd.* **2011**, *509*, 4390–4393.
- (14) Segev, D.; Wei, S.-H. Structure-derived electronic and optical properties of transparent conducting oxides. *Phys. Rev. B: Condens. Matter Mater. Phys.* **2005**, *71*, No. 125129.
- (15) Colston, G.; Myronov, M. Electrical properties of n-type 3C-SiC epilayers in situ doped with extremely high levels of phosphorus. *Semicond. Sci. Technol.* **2018**, 33, No. 114007.
- (16) Crandall, R. S. Electrical Conduction in n-Type Cadmium Sulfide at Low Temperatures. *Phys. Rev.* **1968**, *169*, 577–584.
- (17) Walsh, A.; Da Silva, J. L. F.; Wei, S.-H.; Körber, C.; Klein, A.; Piper, L. F. J.; DeMasi, A.; Smith, K. E.; Panaccione, G.; Torelli, P.; Payne, D. J.; Bourlange, A.; Egdell, R. G. Nature of the Band Gap of In<sub>2</sub>O<sub>3</sub> Revealed by First-Principles Calculations and X-Ray Spectroscopy. *Phys. Rev. Lett.* **2008**, *100*, No. 167402.
- (18) Limpijumnong, S.; Reunchan, P.; Janotti, A.; Van De Walle, C. G. Hydrogen doping in indium oxide: An ab initio study. *Phys. Rev. B: Condens. Matter Mater. Phys.* **2009**, *80*, No. 193202.
- (19) Stevanović, V.; Lany, S.; Ginley, D. S.; Tumas, W.; Zunger, A. Assessing capability of semiconductors to split water using ionization potentials and electron affinities only. *Phys. Chem. Chem. Phys.* **2014**, *16*, 3706–3714.
- (20) Kim, H. J.; Kim, U.; Kim, T. H.; Kim, J.; Kim, H. M.; Jeon, B.-G.; Lee, W.-J.; Mun, H. S.; Hong, K. T.; Yu, J.; Char, K.; Kim, K. H. Physical properties of transparent perovskite oxides (Ba,La)SnO<sub>3</sub> with high electrical mobility. *Phys. Rev. B: Condens. Matter Mater. Phys.* **2012**, *86*, No. 165205.
- (21) van Benthem, K.; Elsässer, C.; French, R. H. Bulk electronic structure of SrTiO<sub>3</sub>: Experiment and theory. *J. Appl. Phys.* **2001**, *90*, 6156–6164
- (22) Tufte, O. N.; Chapman, P. W. Electron Mobility in Semiconducting Strontium Titanate. *Phys. Rev.* **1967**, *155*, 796–802. (23) Dimitrievska, M.; Ivetić, T. B.; Litvinchuk, A. P.; Fairbrother, A.; Miljević, B. B.; Štrbac, G. R.; Pérez Rodríguez, A.; Lukić-Petrović, S. R. Eu3+-Doped Wide Band Gap Zn<sub>2</sub>SnO<sub>4</sub> Semiconductor Nanoparticles: Structure and Luminescence. *J. Phys. Chem. C* **2016**,
- 120, 1887–18894. (24) Ueda, N.; Omata, T.; Hikuma, N.; Ueda, K.; Mizoguchi, H.; Hashimoto, T.; Kawazoe, H. New oxide phase with wide band gap and high electroconductivity, MgIn<sub>2</sub>O<sub>4</sub>. *Appl. Phys. Lett.* **1992**, *61*, 1954–1955.
- (25) Kawazoe, H.; Ueda, K. Transparent Conducting Oxides Based on the Spinel Structure. J. Am. Ceram. Soc. 1999, 82, 3330-3336.
- (26) Özgür, Ü.; Alivov, Y. I.; Liu, C.; Teke, A.; Reshchikov, M. A.; Doğan, S.; Avrutin, V.; Cho, S.-J.; Morkoç, H. A comprehensive review of ZnO materials and devices. *J. Appl. Phys.* **2005**, 98, No. 041301.
- (27) Nagasawa, M.; Shionoya, S. Exciton structure in optical absorption of  $SnO_2$  crystals. *Phys. Lett.* **1966**, 22, 409–410.
- (28) Edwards, P. P.; Porch, A.; Jones, M. O.; Morgan, D. V.; Perks, R. M. Basic materials physics of transparent conducting oxides. *Dalton Trans.* **2004**, 2995.

- (29) Bellal, B.; Hadjarab, B.; Bouguelia, A.; Trari, M. Visible light photocatalytic reduction of water using SrSnO<sub>3</sub> sensitized by CuFeO<sub>2</sub>. *Theor. Exp. Chem.* **2009**, *45*, 172–179.
- (30) Hadjarab, B.; Bouguelia, A.; Trari, M. Synthesis, physical and photo electrochemical characterization of La-doped SrSnO<sub>3</sub>. *J. Phys. Chem. Solids* **2007**, *68*, 1491–1499.
- (31) Pearton, S. J.; Yang, J.; Cary, P. H.; Ren, F.; Kim, J.; Tadjer, M. J.; Mastro, M. A. A review of Ga<sub>2</sub>O<sub>3</sub> materials, processing, and devices. *Appl. Phys. Rev.* **2018**, *5*, No. 011301.
- (32) Lany, S. Defect phase diagram for doping of Ga<sub>2</sub>O<sub>3</sub>. APL Mater. **2018**, 6, No. 046103.
- (33) Yashima, I.; Watanave, H.; Ogisu, T.; Tsukuda, R.; Sato, S. Thermoelectric Properties and Hall Effect of Bi<sub>2</sub>Te<sub>3-x</sub>Se<sub>x</sub> Polycrystal-line Materials Prepared by a Hot Press Method. *Jpn. J. Appl. Phys.* **1998**, 37, 2472–2473.
- (34) Filip, M. R.; Patrick, C. E.; Giustino, F. GW quasiparticle band structures of stibnite, antimonselite, bismuthinite, and guanajuatite. *Phys. Rev. B: Condens. Matter Mater. Phys.* **2013**, 87, No. 205125.
- (35) Hor, Y. S.; Richardella, A.; Roushan, P.; Xia, Y.; Checkelsky, J. G.; Yazdani, A.; Hasan, M. Z.; Ong, N. P.; Cava, R. J. p-type Bi2Se3 for topological insulator and low-temperature thermoelectric applications. *Phys. Rev. B: Condens. Matter Mater. Phys.* 2009, 79, No. 195208.
- (36) Goyal, A.; Gorai, P.; Toberer, E. S.; Stevanović, V. First-principles calculation of intrinsic defect chemistry and self-doping in PbTe. *npj Comput. Mater.* **2017**, *3*, No. 42.
- (37) Ohno, S.; Imasato, K.; Anand, S.; Tamaki, H.; Kang, S. D.; Gorai, P.; Sato, H. K.; Toberer, E. S.; Kanno, T.; Snyder, G. J. Phase Boundary Mapping to Obtain n-type Mg3Sb2-Based Thermoelectrics. *Joule* **2018**, *2*, 141–154.
- (38) Shuai, J.; Wang, Y.; Kim, H. S.; Liu, Z.; Sun, J.; Chen, S.; Sui, J.; Ren, Z. Thermoelectric properties of Na-doped Zintl compound: Mg<sub>3</sub>NaSb<sub>2</sub>. Acta Mater. **2015**, 93, 187–193.
- (39) Zhang, J.; Song, L.; Pedersen, S. H.; Yin, H.; Hung, L. T.; Iversen, B. B. Discovery of high-performance low-cost n-type Mg<sub>3</sub>Sb<sub>2</sub>-based thermoelectric materials with multi-valley conduction bands. *Nat. Commun.* **2017**, *8*, No. 13901.
- (40) Varley, J. B.; Schleife, A.; Janotti, A.; Van De Walle, C. G. Ambipolar doping in SnO. Appl. Phys. Lett. 2013, 103, No. 082118.
- (41) Hosono, H.; Ogo, Y.; Yanagi, H.; Kamiya, T. Bipolar Conduction in SnO Thin Films. *Electrochem. Solid-State Lett.* **2011**, 14, H13.
- (42) Strauss, A. J. Electrical Properties of n-Type GaSb. *Phys. Rev.* **1961**, *121*, 1087–1090.
- (43) Kolezynski, A.; Nieroda, P.; Wojciechowski, K. T. Li doped Mg<sub>2</sub>Si p-type thermoelectric material: Theoretical and experimental study. *Comput. Mater. Sci.* **2015**, *100*, 84–88.
- (44) Nolas, G. S.; Wang, D.; Beekman, M. Transport properties of polycrystalline Mg<sub>2</sub>Si<sub>1-y</sub>Sb<sub>y</sub>. *Phys. Rev. B: Condens. Matter Mater. Phys.* **2007**, 76, No. 235204.
- (45) Duong, A. T.; Nguyen, V. Q.; Duvjir, G.; Duong, V. T.; Kwon, S.; Song, J. Y.; Lee, J. K.; Lee, J. E.; Park, S.; Min, T.; Lee, J.; Kim, J.; Cho, S. Achieving ZT=2.2 with Bi-doped n-type SnSe single crystals. *Nat. Commun.* **2016**, *7*, No. 13713.
- (46) Kumagai, Y.; Tsunoda, N.; Oba, F. Point Defects and p-Type Doping in ScN from First Principles. *Phys. Rev. Appl.* **2018**, *9*, No. 034019.
- (47) Deng, R.; Ozsdolay, B. D.; Zheng, P. Y.; Khare, S. V.; Gall, D. Optical and transport measurement and first-principles determination of the ScN band gap. *Phys. Rev. B: Condens. Matter Mater. Phys.* **2015**, 91, No. 045104.
- (48) Saha, B.; Garbrecht, M.; Perez-Taborda, J. A.; Fawey, M. H.; Koh, Y. R.; Shakouri, A.; Martin-Gonzalez, M.; Hultman, L.; Sands, T. D. Compensation of native donor doping in ScN: Carrier concentration control and p-type ScN. *Appl. Phys. Lett.* **2017**, *110*, No. 252104.
- (49) Fioretti, A. N.; Schwartz, C. P.; Vinson, J.; Nordlund, D.; Prendergast, D.; Tamboli, A. C.; Caskey, C. M.; Tuomisto, F.; Linez, F.; Christensen, S. T.; Toberer, E. S.; Lany, S.; Zakutayev, A.

Understanding and control of bipolar self-doping in copper nitride. *J. Appl. Phys.* **2016**, *119*, No. 181508.

- (50) Vidal, J.; Lany, S.; D'Avezac, M.; Zunger, A.; Zakutayev, A.; Francis, J.; Tate, J. Band-structure, optical properties, and defect physics of the photovoltaic semiconductor SnS. *Appl. Phys. Lett.* **2012**, *100*, No. 032104.
- (51) Xiao, Z.; Ran, F.-Y.; Hosono, H.; Kamiya, T. Route to n-type doping in SnS. *Appl. Phys. Lett.* **2015**, *106*, No. 152103.
- (52) Bugajski, M.; Lewandowski, W. Concentration-dependent absorption and photoluminescence of n-type InP. *J. Appl. Phys.* **1985**, *57*, 521–530.
- (53) Neave, J. H.; Dobson, P. J.; Harris, J. J.; Dawson, P.; Joyce, B. A. Silicon doping of MBE-grown GaAs films. *Appl. Phys. A: Solids Surf.* **1983**, 32, 195–200.
- (54) Sun, S.; Armour, E.; Zheng, K.; Schaus, C. Zinc and tellurium doping in GaAs and AlGaAs grown by MOCVD. *J. Cryst. Growth* **1991**, *113*, 103–112.
- (55) Su, C.-H. Energy band gap, intrinsic carrier concentration, and Fermi level of CdTe bulk crystal between 304 and 1067 K. *J. Appl. Phys.* **2008**, *103*, No. 084903.
- (56) Segall, B.; Lorenz, M. R.; Halsted, R. E. Electrical Properties of n-Type CdTe. *Phys. Rev.* **1963**, *129*, 2471–2481.
- (57) Nagaoka, A.; Kuciauskas, D.; McCoy, J.; Scarpulla, M. A. High p-type doping, mobility, and photocarrier lifetime in arsenic-doped CdTe single crystals. *Appl. Phys. Lett.* **2018**, *112*, No. 192101.
- (58) Simpson, J.; Wallace, J. M.; Wang, S. Y.; Stewart, H.; Hunter, J. J.; Adams, S. J.; Prior, K. A.; Cavenett, B. C. N-type doping of molecular beam epitaxial zinc selenide using an electrochemical iodine cell. *Semicond. Sci. Technol.* **1992**, *7*, 464–466.
- (59) Van De Walle, C. G.; Laks, D. B.; Neumark, G. F.; Pantelides, S. T. First-principles calculations of solubilities and doping limits: Li, Na, and N in ZnSe. *Phys. Rev. B: Condens. Matter Mater. Phys.* **1993**, 47, 9425–9434.
- (60) Ueno, K.; Fudetani, T.; Arakawa, Y.; Kobayashi, A.; Ohta, J.; Fujioka, H. Electron transport properties of degenerate n-type GaN prepared by pulsed sputtering. *APL Mater.* **2017**, *5*, No. 126102.
- (61) Tsu, R.; Howard, W. E.; Esaki, L. Optical and Electrical Properties and Band Structure of GeTe and SnTe. *Phys. Rev.* **1968**, 172, 779–788.
- (62) Tenga, A.; Lidin, S.; Belieres, J.-P.; Newman, N.; Wu, Y.; Haeussermann, U. ChemInform Abstract: Metastable Cd<sub>4</sub>Sb<sub>3</sub>: A Complex Structured Intermetallic Compound with Semiconductor Properties. *ChemInform* **2009**, *40*, 15564–15572.
- (63) Hrubý, A.; Kubelík, I.; Štourač, L. Electrical conductivity and thermoelectric power of heavily doped P-type CdSb. *Czech. J. Phys.* **1965**, *15*, 740–746.
- (64) Böttger, P. H. M.; Pomrehn, G. S.; Snyder, G. J.; Finstad, T. G. Doping of p-type ZnSb: Single parabolic band model and impurity band conduction. *Phys. Status Solidi A* **2011**, 208, 2753–2759.
- (65) Liu, X.; Chen, J.; Luo, M.; Leng, M.; Xia, Z.; Zhou, Y.; Qin, S.; Xue, D.-J.; Lv, L.; Huang, H.; Niu, D.; Tang, J. Thermal Evaporation and Characterization of Sb<sub>2</sub>Se<sub>3</sub> Thin Film for Substrate Sb2Se<sub>3</sub> /CdS Solar Cells. ACS Appl. Mater. Interfaces 2014, 6, 10687–10695.
- (66) Chen, C.; Bobela, D. C.; Yang, Y.; Lu, S.; Zeng, K.; Ge, C.; Yang, B.; Gao, L.; Zhao, Y.; Beard, M. C.; Tang, J. Characterization of basic physical properties of Sb<sub>2</sub>Se<sub>3</sub> and its relevance for photovoltaics. *Front. Optoelectron.* **2017**, *10*, 18–30.
- (67) Shay, J. L.; Tell, B.; Buehler, E.; Wernick, J. H. Band Structure of ZnGeP<sub>2</sub> and ZnSiP<sub>2</sub>-Ternary Compounds with Pseudodirect Energy Gaps. *Phys. Rev. Lett.* **1973**, *30*, 983–986.
- (68) Heinemann, M.; Eifert, B.; Heiliger, C. Band structure and phase stability of the copper oxides Cu2O, CuO and Cu<sub>4</sub>O<sub>3</sub>. *Phys. Rev. B: Condens. Matter Mater. Phys.* **2013**, 87, No. 115111.
- (69) Bergum, K.; Riise, H. N.; Gorantla, S.; Lindberg, P. F.; Jensen, I. J. T.; Gunnæs, A. E.; Galeckas, A.; Diplas, S.; Svensson, B. G.; Monakhov, E. Improving carrier transport in Cu<sub>2</sub>O thin films by rapid thermal annealing. *J. Phys.: Condens. Matter* **2018**, *30*, No. 075702.
- (70) Ueda, K.; Hosono, H.; Hamada, N. Energy band structure of LaCuOCh (Ch = S, Se and Te) calculated by the full-potential

linearized augmented plane-wave method. J. Phys.: Condens. Matter 2004, 16, 5179-5186.

- (71) Barati, A.; Klein, A.; Jaegermann, W. Deposition and characterization of highly p-type antimony doped ZnTe thin films. *Thin Solid Films* **2009**, *517*, 2149–2152.
- (72) Hiramatsu, H.; Ueda, K.; Ohta, H.; Hirano, M.; Kamiya, T.; Hosono, H. Degenerate p-type conductivity in wide-gap LaCuOSSe epitaxial films. *Appl. Phys. Lett.* **2003**, *82*, 1048–1050.
- (73) Ahn, D.; Park, S.-H. Cuprous halides semiconductors as a new means for highly efficient light-emitting diodes. *Sci. Rep.* **2016**, *6*, No. 20718.
- (74) Yang, C.; Kneiß, M.; Lorenz, M.; Grundmann, M. Room-temperature synthesized copper iodide thin film as degenerate p-type transparent conductor with a boosted figure of merit. *Proc. Natl. Acad. Sci. U.S.A.* **2016**, *113*, 12929–12933.
- (75) Tate, J.; Ju, H. L.; Moon, J. C.; Zakutayev, A.; Richard, A. P.; Russell, J.; McIntyre, D. H. Origin of p-type conduction in single crystal CuAlO<sub>2</sub>. *Phys. Rev. B: Condens. Matter Mater. Phys.* **2009**, 80, No. 165206.
- (76) Kawazoe, H.; Yasukawa, M.; Hyodo, H.; Kurita, M.; Yanagi, H.; Hosono, H. P-type electrical conduction in transparent thin films of CuAlO<sub>2</sub>. *Nature* **1997**, 389, 939–942.
- (77) Ohta, H.; Orita, M.; Hirano, M.; Yagi, I.; Ueda, K.; Hosono, H. Electronic structure and optical properties of SrCu<sub>2</sub>O<sub>2</sub>. *J. Appl. Phys.* **2002**, *91*, 3074–3078.
- (78) Kudo, A.; Yanagi, H.; Hosono, H.; Kawazoe, H. SrCu<sub>2</sub>O<sub>2</sub>: A ptype conductive oxide with wide band gap. *Appl. Phys. Lett.* **1998**, 73, 220–222.
- (79) Akasaki, I. Nobel Lecture: Fascinated journeys into blue light. Rev. Mod. Phys. 2015, 87, 1119–1131.
- (80) Amano, H. Nobel Lecture: Growth of GaN on sapphire via low-temperature deposited buffer layer and realization of p-type GaN by Mg doping followed by low-energy electron beam irradiation. *Rev. Mod. Phys.* **2015**, *87*, 1133–1138.
- (81) Nakamura, S. Nobel Lecture: Background story of the invention of efficient blue InGaN light emitting diodes. *Rev. Mod. Phys.* **2015**, 87, 1139–1151.
- (82) Janotti, A.; Van de Walle, C. G. Fundamentals of zinc oxide as a semiconductor. *Rep. Prog. Phys.* **2009**, *72*, No. 126501.
- (83) Hosono, H.; Paine, D. C.; Ginley, D. In *Handbook of Transparent Conductors*; Ginley, D. S., Ed.; Springer US: Boston, MA, 2011.
- (84) King, P. D. C.; Veal, T. D. Conductivity in transparent oxide semiconductors. *J. Phys.: Condens. Matter* **2011**, 23, No. 334214.
- (85) Lany, S.; Zunger, A. Polaronic hole localization and multiple hole binding of acceptors in oxide wide-gap semiconductors. *Phys. Rev. B* **2009**, *80*, No. 085202.
- (86) Scanlon, D. O.; Watson, G. W. On the possibility of p-type SnO<sub>2</sub>. *J. Mater. Chem.* **2012**, *22*, 25236–25245.
- (87) Goyal, A.; Stevanović, V. Metastable rocksalt ZnO is p-type dopable. *Phys. Rev. Mater.* **2018**, 2, No. 084603.
- (88) Tamaki, H.; Sato, H. K.; Kanno, T. Isotropic Conduction Network and Defect Chemistry in Mg<sub>3</sub>Sb<sub>2</sub>-Based Layered Zintl Compounds with High Thermoelectric Performance. *Adv. Mater.* **2016**, 28, 10182–10187.
- (89) Ohno, S.; Imasato, K.; Anand, S.; Tamaki, H.; Kang, S. D.; Gorai, P.; Sato, H. K.; Toberer, E. S.; Kanno, T.; Snyder, G. J. Phase Boundary Mapping to Obtain n-type Mg3Sb2-Based Thermoelectrics. *Joule* 2018, 2, 141–154.
- (90) Alberi, K.; Nardelli, M. B.; Zakutayev, A.; Mitas, L.; Curtarolo, S.; Jain, A.; Fornari, M.; Marzari, N.; Takeuchi, I.; Green, M. L.; Kanatzidis, M.; Toney, M. F.; Butenko, S.; Meredig, B.; Lany, S.; Kattner, U.; Davydov, A.; Toberer, E. S.; Stevanovic, V.; Walsh, A.; Park, N.-G.; Aspuru-Guzik, A.; Tabor, D. P.; Nelson, J.; Murphy, J.; Setlur, A.; Gregoire, J.; Li, H.; Xiao, R.; Ludwig, A.; Martin, L. W.; Rappe, A. M.; Wei, S.-H.; Perkins, J. The 2019 materials by design roadmap. *J. Phys. D: Appl. Phys.* 2018, 52, No. 013001.

- (91) Gorai, P.; Stevanović, V.; Toberer, E. S. Computationally guided discovery of thermoelectric materials. *Nat. Rev. Mater.* **2017**, *2*, No. 17053.
- (92) Gorai, P.; McKinney, R. W.; Haegel, N. M.; Zakutayev, A.; Stevanovic, V. A computational survey of semiconductors for power electronics. *Energy Environ. Sci.* **2019**, 3338.
- (93) Zunger, A. Practical doping principles. Appl. Phys. Lett. 2003, 83, 57-59.
- (94) Schleife, A.; Fuchs, F.; Rödl, C.; Furthmüller, J.; Bechstedt, F. Branch-point energies and band discontinuities of III-nitrides and III-/II-oxides from quasiparticle band-structure calculations. *Appl. Phys. Lett.* **2009**, *94*, No. 012104.
- (95) Woods-Robinson, R.; Broberg, D.; Faghaninia, A.; Jain, A.; Dwaraknath, S. S.; Persson, K. A. Assessing High-Throughput Descriptors for Prediction of Transparent Conductors. *Chem. Mater.* **2018**, *30*, 8375–8389.
- (96) Freysoldt, C.; Grabowski, B.; Hickel, T.; Neugebauer, J.; Kresse, G.; Janotti, A.; Van de Walle, C. G. First-principles calculations for point defects in solids. *Rev. Mod. Phys.* **2014**, *86*, 253–305.
- (97) Lany, S.; Zunger, A. Accurate prediction of defect properties in density functional supercell calculations. *Modell. Simul. Mater. Sci. Eng.* **2009**, *17*, No. 084002.
- (98) Gorai, P.; Ortiz, B. R.; Toberer, E. S.; Stevanović, V. Investigation of n-type doping strategies for Mg<sub>3</sub>Sb<sub>2</sub>. *J. Mater. Chem. A* **2018**, *6*, 13806–13815.
- (99) Chern, G.-W.; Barros, K.; Batista, C. D.; Kress, J. D.; Kotliar, G. Mott Transition in a Metallic Liquid: Gutzwiller Molecular Dynamics Simulations. *Phys. Rev. Lett.* **2017**, *118*, No. 226401.
- (100) Varley, J. B.; Samanta, A.; Lordi, V. Descriptor-Based Approach for the Prediction of Cation Vacancy Formation Energies and Transition Levels. *J. Phys. Chem. Lett.* **2017**, *8*, 5059–5063.
- (101) Verma, A. S.; Bhardwaj, S. R. Correlation between ionic charge and ground-state properties in rocksalt and zinc blende structured solids. *J. Phys.: Condens. Matter* **2006**, *18*, 8603–8612.
- (102) Wacke, S.; Górecki, T.; Górecki, C.; Książek, K. Relations between the cohesive energy, atomic volume, bulk modulus and sound velocity in metals. *J. Phys.: Conf. Ser.* **2011**, 289, No. 012020.
- (103) Deml, A. M.; Holder, A. M.; O'Hayre, R. P.; Musgrave, C. B.; Stevanović, V. Intrinsic Material Properties Dictating Oxygen Vacancy Formation Energetics in Metal Oxides. *J. Phys. Chem. Lett.* **2015**, *6*, 1948–1953.
- (104) Lide, R. D., Ed.CRC Handbook of Chemistry and Physics, 90th ed.; CRC Press: Boca Raton, FL, 2009.
- (105) Kramida, A.; Ralchenko, Y.; Reader, J.; NIST ASD Team. *NIST Atomic Spectra Database*, version 5.6.1 [Online]; National Institute of Standards and Technology: Gaithersburg, MD, 2018. Available: https://physics.nist.gov/asd (Jan 31, 2016).
- (106) Lany, S. Semiconducting transition metal oxides. J. Phys.: Condens. Matter 2015, 27, No. 283203.
- (107) Zhang, S. B.; Wei, S.-H.; Zunger, A. Microscopic Origin of the Phenomenlogical Equilibrium "Doping Limit Rule" in n-Type III-V Semiconductors. *Phys. Rev. Lett.* **2000**, *84*, 1232–1235.
- (108) Walukiewicz, W. Mechanism of Fermi-level stabilization in semiconductors. *Phys. Rev. B: Condens. Matter Mater. Phys.* **1988**, *37*, 4760–4763.
- (109) Robertson, J.; Clark, S. J. Limits to doping in oxides. *Phys. Rev. B: Condens. Matter Mater. Phys.* **2011**, 83, No. 075205.
- (110) Tardío, M. M.; Ramírez, R.; González, R.; Chen, Y. p-type semiconducting properties in lithium-doped MgO single crystals. *Phys. Rev. B: Condens. Matter Mater. Phys.* **2002**, *66*, No. 134202.
- (111) McCluskey, M. D.; Corolewski, C. D.; Lv, J.; Tarun, M. C.; Teklemic hael, S. T.; Walter, E. D.; Norton, M. G.; Harrison, K. W.; Ha, S. Acceptors in ZnO. *J. Appl. Phys.* **2015**, *117*, No. 112802.
- (112) Gorai, P.; Goyal, A.; Toberer, E. S.; Stevanović, V. A simple chemical guide for finding novel n-type dopable Zintl pnictide thermoelectric materials. *J. Mater. Chem. A* **2019**, *7*, 19385–19395.

- (113) Goyal, A.; Gorai, P.; Peng, H.; Lany, S.; Stevanović, V. A computational framework for automation of point defect calculations. *Comput. Mater. Sci.* **2017**, *130*, 1–9.
- (114) Stevanović, V.; Lany, S.; Zhang, X.; Zunger, A. Correcting density functional theory for accurate predictions of compound enthalpies of formation: Fitted elemental-phase reference energies. *Phys. Rev. B: Condens. Matter Mater. Phys.* **2012**, *85*, No. 115104.
- (115) Monkhorst, H. J.; Pack, J. D. Special points for Brillouin-zone integrations. *Phys. Rev. B: Condens. Matter Mater. Phys.* **1976**, 13, 5188–5192.
- (116) Peng, H.; Scanlon, D. O.; Stevanovic, V.; Vidal, J.; Watson, G. W.; Lany, S. Convergence of density and hybrid functional defect calculations for compound semiconductors. *Phys. Rev. B: Condens. Matter Mater. Phys.* **2013**, 88, No. 115201.
- (117) Hedin, L. New Method for Calculating the One-Particle Greenas Function with Application to the Electron-Gas Problem. *Phys. Rev.* **1965**, *139*, A796–A823.
- (118) Heyd, J.; Scuseria, G. E.; Ernzerhof, M. Hybrid functionals based on a screened Coulomb potential. *J. Chem. Phys.* **2003**, *118*, 8207–8215.
- (119) Heyd, J.; Scuseria, G. E.; Ernzerhof, M. Erratum: "Hybrid functionals based on a screened Coulomb potential" [J. Chem. Phys. 118, 8207 (2003)]. *J. Chem. Phys.* 2006, 124, No. 219906.
- (120) Biswas, K.; Lany, S. Energetics of quaternary III-V alloys described by incorporation and clustering of impurities. *Phys. Rev. B: Condens. Matter Mater. Phys.* **2009**, *80*, No. 115206.